EDGE ARTICLE

Towards metal–organic framework based field effect chemical sensors: UiO-66-NH₂ for nerve agent detection†

I. Stassen,[ab] B. Bueken,[a] H. Reinsch,[c] J. F. M. Oudenhoven,[d] D. Wouters,[d] J. Hajek,[e] V. Van Speybroeck,[e] N. Stock,[c] P. M. Vereecken,[ab] R. Van Schaijk,[d] D. De Vos[a] and R. Ameloot*[a]

We present a highly sensitive gas detection approach for the infamous 'nerve agent' group of alkyl phosphonate compounds. Signal transduction is achieved by monitoring the work function shift of metal–organic framework UiO-66-NH₂ coated electrodes upon exposure to ppb-level concentrations of a target simulant. Using the Kelvin probe technique, we demonstrate the potential of electrically insulating MOFs for integration in field effect devices such as ChemFETs: a three orders of magnitude improvement over previous work function-based detection of nerve agent simulants. Moreover, the signal is fully reversible both in dry and humid conditions, down to low ppb concentrations. Comprehensive investigation of the interactions that lead towards this high sensitivity points towards a series of confined interactions between the analyte and the pore interior of UiO-66-NH₂.

Introduction

Detection of chemical warfare agents is both an unsolved challenge and a current need,[1] particularly in the context of terrorism threats. Volatile alkyl phosphonate nerve agents are a nefarious group of compounds that inhibit acetylcholinesterase (AChE), resulting in asphyxiation even at very low levels of exposure.[2] For example, the 10 min acute exposure guideline limit (AEGL-2) for sarin (*O*-isopropyl methylphosphonofluoridate, GB) is merely 15 ppb.[3] This compound has become infamous because of its use in the 1995 Tokyo subway attack and Gulf wars.[4] Dimethyl methylphosphonate (DMMP) is a widely used and relatively safe to handle sarin simulant (Fig. 1a). State-of-the-art metal oxide gas sensors display DMMP detection limits that are tenfold higher than required for sarin.[5,6] The application of designer polymer adsorbent films combined with optical and micro-electromechanical transducers resulted in prototype sensors able to detect low-ppb DMMP levels under idealized conditions.[7–10]

Nevertheless, improved sensing materials and transducer mechanisms are still essential to elevate reliability, selectivity and response kinetics to a level suitable for commercial implementation.[11,12] Work function-based gas sensors, such as chemically sensitive field effect transistors (ChemFETs), transduce the interaction of analyte molecules with the gate electrode of a metal–insulator–semiconductor FET to a change in source-drain current. The principle underpinning signal transduction in ChemFETs is chemical modulation of the gate electrode work function through a change in surface functionalization or adsorbed surface species.[13,14] In practical devices, this work function modulation is observed as a shift in contact potential difference (CPD) relative to a reference electrode. ChemFETs are interesting for real-world applications because they are robust, highly sensitive and compatible with readily scalable, inexpensive CMOS fabrication.[12,15]

Metal–organic frameworks (MOFs) are a class of crystalline porous materials that consist of metal-containing nodes connected by multitopic organic linkers.[16,17] These tailorable, high specific surface area materials show outstanding potential in catalysis,[18] gas storage[19] and molecular separations.[20] Recently, interest in integrating these materials in devices has increased rapidly,[21–24] for instance as selective adsorbent layers in various types of chemical sensors.[25–27] Although MOF-based sensors for alkyl phosphonates have not yet been developed, previous work demonstrated the suitability of MOFs as adsorptive concentrators for this family of compounds.[28,29] Recent illustrations of MOF-catalyzed decomposition of nerve gas simulants further underline the high affinity that framework building blocks such as metal oxide clusters can have for alkyl phosphonates.[30–32] The

ᵃCentre for Surface Chemistry and Catalysis, KU Leuven – University of Leuven, Celestijnenlaan 200F, B-3001 Leuven, Belgium. E-mail: rob.ameloot@biw.kuleuven.be
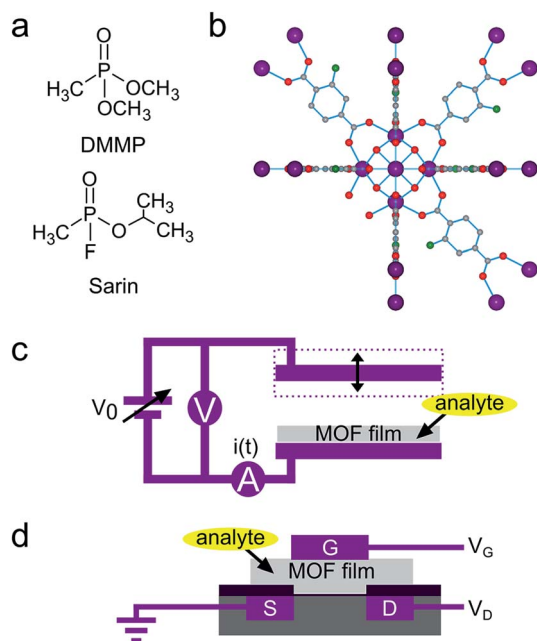
ᵇImec, Kapeldreef 75, B-3001 Leuven, Belgium

ᶜInstitute of Inorganic Chemistry, Christian-Albrechts-University Kiel, Max-Eyth-Straße 2, 24118 Kiel, Germany

ᵈHolst Centre/imec, High Tech Campus 31, 5656 AE, Eindhoven, The Netherlands

ᵉCenter for Molecular Modeling, Ghent University, Technologiepark 903, B-9052 Zwijnaarde, Belgium

Fig. 1 Field effect DMMP sensing strategy using a MOF adsorbent film. (a) Structure of sarin and the simulant DMMP. (b) Representation of UiO-66-NH₂, showing the $[Zr_6O_4(OH)_4]^{12+}$ inorganic clusters, 2-aminoterephthalate organic linkers, as well as a missing linker defect site on the cluster. Atom colors: Zr (purple), O (red), C (grey) and N (green). H atoms are omitted for clarity. (c) Schematic representation of the Kelvin probe configuration used in this study. The MOF film is deposited on a stationary electrode that is electrically connected to an oscillating reference electrode. During sensing experiments, the analyte flows between both electrodes. (d) Schematic representation of suspended gate ChemFET, which is a miniaturized counterpart of the Kelvin probe and a potential real-world implementation.

$[Zr_6O_4(OH)_4]^{12+}$ cluster that is embedded in carboxylate-linked UiO-66 type materials (Fig. 1b)[33] has been of specific interest because of its remarkably high activity towards phosphate ester hydrolysis. The catalytically active site on this cluster is considered a biomimetic analogue of the bridged hydroxy ligand in the phosphotriesterase enzyme.[34] Inspired by this high-affinity site, we investigated the potential of these non-conductive hybrid materials for implementation in ChemFET nerve gas sensors, in a similar fashion as high-affinity enzymes have been used in FET sensors.[35]

Herein, we report high CPD shifts of UiO-66-NH₂ covered electrodes upon exposure to DMMP concentrations down to 3 ppb in a Kelvin probe configuration. This response is generated by strong DMMP adsorption in the well-defined MOF pores, in proximity to the interface of the electrically insulating MOF and the electrode. The extrapolated (3σ) limit of detection for DMMP of the demonstrated system is 0.3 ± 0.1 ppb and the observed response time is 1.9 ± 1.3 min. This study is an important step towards implementation of MOFs in ChemFET sensors.

Results and discussion

Kelvin probe DMMP sensing using UiO-66-NH₂

The Kelvin probe technique is a well-established tool to measure the CPD between a stationary electrode and an oscillating reference electrode.[13] The CPD consists of a bulk contribution, associated with the Fermi level of the electrodes, and a surface contribution, associated with the work function. The work function is connected to the chemical potential at the electrode surface, which is influenced by adsorption of molecules. At low analyte concentrations, this effect can be amplified by functionalizing the electrode with an adsorbent layer, to accumulate target molecules in proximity to the electrode surface.[36,37] Practically, a balancing potential $V_b = -CPD$ is determined through biasing both electrodes respective to each other, thus zeroing the current that flows due to the oscillation of the capacitance (Fig. 1c). Kelvin probe transducers are not used as commercial sensors because of the non-scalability of the instrumentation. However, ChemFETs transduce the same analyte-induced work function shifts that are the basis of signals measured by the Kelvin probe. As the CPD change upon analyte exposure is an intensive surface property, the Kelvin probe technique is an effective macroscopic screening tool for sensing materials to be implemented in miniaturized ChemFETs (Fig. 1d).[12,38]

UiO-66-NH₂ (Fig. 1b) was selected because of its superior catalytic activity in the decomposition of phosphonates.‡ This high activity has been linked to the amino moiety that can accept protons from nearby $[Zr_6O_4(OH)_4]^{12+}$ clusters and thereby induces stronger, possibly bidentate, adsorption of the phosphonates.[39] UiO-66-NH₂ powder was drop-casted on a silicon electrode and exposed to different DMMP concentrations in a flow cell (Fig. 2a and b). Real-time Kelvin probe monitoring showed CPD shifts of tens of millivolts. These signals were reversible and consistent between repeated exposures (Fig. 2c). Moreover, the signal-to-noise ratio remained significant even at concentrations down to 3 ppb, the lowest reachable concentration for our dosing system (Fig. 2d).

The average response time t_{r90} and decay time t_{d90} observed for the signal over the measured concentration range was 1.9 ± 1.3 min and 5.7 ± 3.5 min respectively (Fig. S3†). The observed response time is in line with previous low concentration DMMP sensing studies using adsorptive sensing materials.[40–42] The relatively slow decay of the signal indicates that desorption is rate-limiting for the signal due to high affinity of the sensing material for DMMP. Mass transport limitation through the relatively narrow pore aperture size of the MOF (*ca.* 0.5 nm) is another potential factor of influence.

Plotting the CPD shift signal at equilibrium in function of the DMMP concentration yields a non-linear relationship that can be fitted by an empirical Freundlich adsorption isotherm of the form $|\Delta CPD| = K\sqrt[n]{C}$, with C the DMMP concentration in ppb and K and n fitted parameters (Fig. 2e). The extrapolated limit of detection (LOD) of this fitted relationship ($K = 7.98 \pm 1.06$, $n = 2.18 \pm 0.22$, $R^2 = 0.990$) is 0.3 ± 0.1 ppb for a 3σ noise level of 4.2 mV. To the best of our knowledge, this is the lowest LOD demonstrated to date for Kelvin probe gas sensing.[43] Of all reported DMMP sensor types, only a capacitive ultrasonic transducer performed significantly better when used in vibration-isolated conditions (0.05 ppb LOD, 2 min t_{r90}).[8] Linear interpolation of the response in the range of the AEGL-2 level for sarin results in a sensitivity of 0.78 mV ppb⁻¹, which
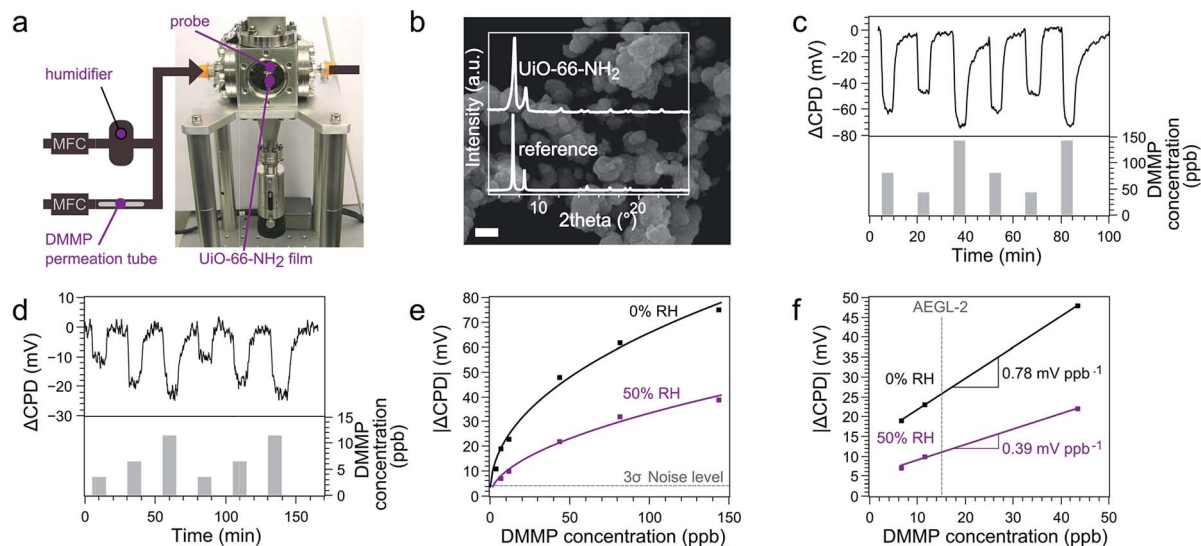
Fig. 2 Kelvin probe DMMP sensing measurements. (a) Schematic representation of the experimental setup: two air flows are mixed to obtain different DMMP concentrations in the Kelvin probe measurement cell. RH is controlled by a humidifier system. (b) SEM image of drop-casted UiO-66-NH$_2$ film. Scale bar: 1 μm. Inset, experimental and reference X-ray diffraction patterns. (c and d) CPD responses at 0% RH for DMMP concentrations in the ranges 40–150 ppb and 3–15 ppb, respectively. (e) Freundlich isotherm fit of the CPD response, at 0% and 50% RH. (f) Linearized fit of the CPD response in the range of the AEGL-2 level for sarin.

corresponds to a signal resolution of 1.28 ppb mV^{-1}. This sensitivity and LOD are at least three orders of magnitude better than reported in previous work on MOF work function-based sensing.[44,45] These results underline how the periodic high-affinity adsorption sites in MOF pores can be judiciously matched with specific target analytes to achieve detection at low concentrations.

### Influence of humidity on the sensing response

An often overlooked but nevertheless decisive parameter for the robustness and reliability of a sensing material is its interaction with humidity. The CPD response to a 50% relative humidity (RH) background was measured to simulate a situation more representative of real-world applications. The stable and reversible response resulting from water uptake, around 100 mV at 50% RH (Fig. S4 and S5†), confirms the expected water stability of the UiO-66-NH$_2$ material.[46] Remarkably, this response is similar in range as for ppb-range DMMP levels, despite the 5 orders of magnitude higher water concentration. This observation indicates that the work function of the electrode is influenced to a much lower extent by the adsorption of water in the MOF pores compared to DMMP. As indicated by a previous study,[45] the higher CPD response towards DMMP compared to water points towards stronger adsorptive interactions of the former. Consistently, when DMMP was introduced under 50% RH, responses of similar magnitude as under dry conditions were observed. The extrapolated LOD for DMMP at this RH is 2.0 ± 0.5 ppb (K = 2.89 ± 0.42, n = 1.88 ± 0.15) and the sensitivity and signal resolution are 0.39 mV ppb^{-1} and 2.56 ppb mV^{-1}, respectively. This experiment shows that the sensitivity to DMMP is still very high, even when the pores are saturated with water (Fig. S6†). These results are remarkable

and can only be explained by a much higher affinity of the adsorption sites for DMMP than for water.

Elucidating DMMP adsorption in the cavities of UiO-66-NH$_2$

A ppm-range DMMP UiO-66-NH$_2$ adsorption isotherm was measured at 300 K (saturation at 1265 ppm).[47] This isotherm clearly reveals the high affinity of UiO-66-NH$_2$ for DMMP, apparent from the significant uptake at low concentrations (Fig. 3a). The volumetric partition coefficient ($P_{MOF/air}$), defined as the ratio of DMMP per volume in the adsorbent and in vapor phase, is in the order of 10^6 in the concentration region below 15 ppm. This partition coefficient is two to three orders of magnitude higher than those observed for DMMP sensing polymers,[48] and matches the best-performing sensing material to date (DKAP, proprietary polymer, Sandia National Lab).[8,49] Decreasing affinity for DMMP is observed from roughly 0.31 adsorbed DMMP molecules per zirconium atom onwards, which corresponds to 1.9 DMMP molecules per $[Zr_6O_4(OH)_4]^{12+}$ cluster. This number agrees well with the number of missing linker defects estimated based on thermogravimetric analysis (Fig. S7†), and indicates that these defects are likely related with the highest-affinity DMMP adsorption sites.

Two DMMP loaded UiO-66-NH$_2$ samples were further analyzed, at a loading of 1.2 DMMP per cluster (MOF$_{DMMP-L}$) and at a loading that is 5 times higher (MOF$_{DMMP-H}$). Together with a non-loaded UiO-66-NH$_2$ reference sample, these samples were analyzed using gravimetric temperature programmed desorption (TPD) and attenuated total reflectance Fourier transform infrared spectroscopy (ATR-FTIR). TPD reveals desorption of DMMP in the 400–450 K temperature range for MOF$_{DMMP-L}$ (Fig. 3b). Desorption occurs at slightly lower temperature than the well-described cluster dehydroxylation
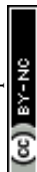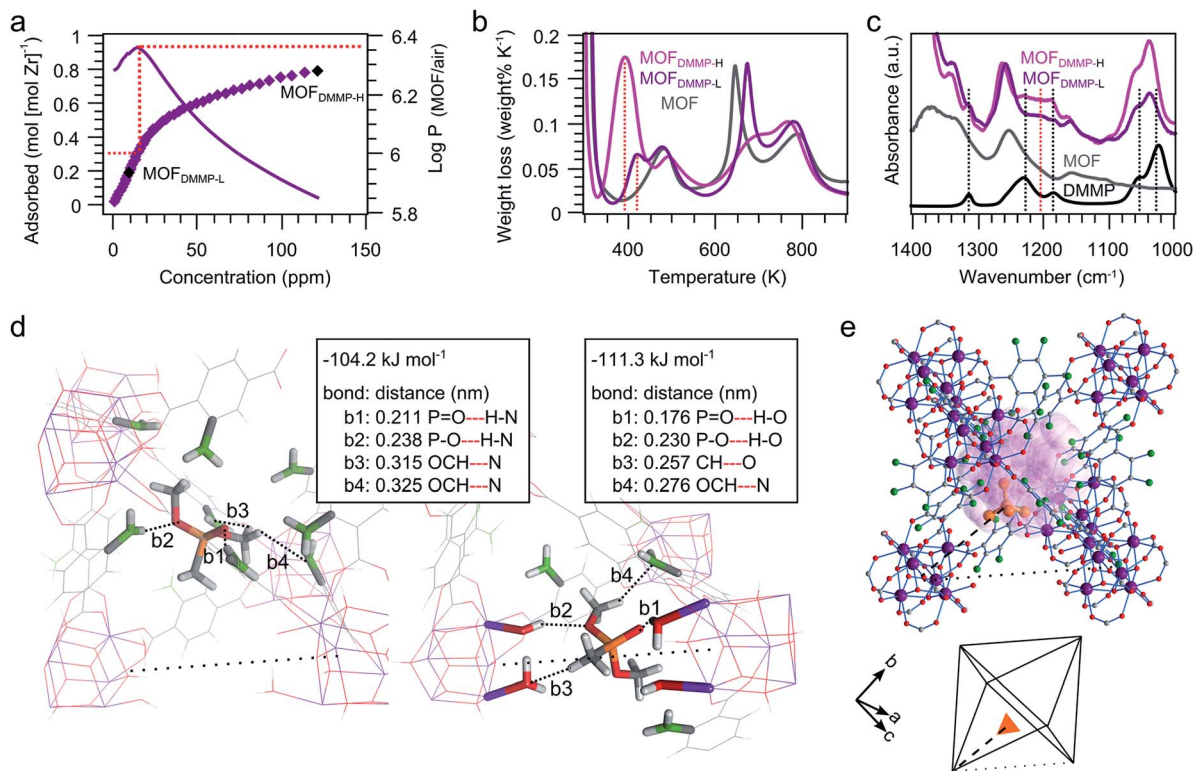
Fig. 3 DMMP adsorption in UiO-66-NH$_2$. (a) DMMP adsorption isotherm at 300 K. The isotherm data are shown as diamonds. The smooth line displays the volumetric partition coefficient. Two samples were analyzed further, which are annotated as MOF$_{DMMP-L}$ (L, for low loading) and MOF$_{DMMP-H}$ (H, for high loading) on the isotherm. The dotted red line indicates the loading corresponding to the highest partition coefficient. (b) TPD data for MOF$_{DMMP-L}$ and MOF$_{DMMP-H}$ displayed together with a reference UiO-66-NH$_2$ sample. The dotted red lines highlight the peaks corresponding to desorption of DMMP. (c) ATR-FTIR spectra for MOF$_{DMMP-L}$ and MOF$_{DMMP-H}$ displayed together with reference UiO-66-NH$_2$ and liquid DMMP samples. The dotted lines highlight bands corresponding to DMMP (black) and DMMP–cluster interaction (red). (e) Adsorption energy predicted for DMMP by periodic DFT calculations, two nearly energetically equivalent adsorption sites were found, one in the octahedral cage (left) and one in the position of the missing linker defect (right). Key interactions between DMMP and the framework (b1–b4) are allocated for both sites based on the observed center-to-center atomic distances. (d) Rietveld refined position of the tetrahedral phosphorus center of DMMP in the octahedral cage of UiO-66-NH$_2$ based on powder X-ray diffraction (MOF$_{DMMP-L}$). The purple cloud represents 48 symmetrically equivalent positions that are consistent with the refinement. The orange tetrahedron, corresponding missing linker (dotted line), interacting cluster (dashed line) and schematic wireframe representation illustrate a specific case that resembles the position of adsorption site simulated by DFT. Atom colors: Zr (purple), O (red), C (dark grey), H (light grey), P (orange) and N (green).

(450–520 K),[50] but at significantly higher temperature than a liquid DMMP reference run (full evaporation below 370 K). This observation points toward relatively strong physisorption, which corresponds with the high affinity and fully reversible behavior observed in Kelvin probe sensing. This observation is further confirmed by ATR-FTIR (Fig. 3c). The P=O stretching mode is sensitive to nucleophilic interactions of the oxygen atom, which are accompanied by a loss of electron density of the double bond and a shift towards lower wavenumbers. This effect is clearly demonstrated by a shift between the vapor (1276 cm^{-1})[51] and liquid phase (1230 cm^{-1}). In MOF$_{DMMP-L}$, this P=O band is broadened and shifted to even lower (1205 cm^{-1}) wavenumbers, consistent with a strong nucleophilic interaction with the pore interior. In contrast, the measurements on MOF$_{DMMP-H}$ show that excess DMMP, adsorbed after saturation of the strongly interacting sites, behaves similar to liquid DMMP. Desorption is observed mainly in the 350–400 K temperature range and the position of the broad P=O stretching band perfectly matches the liquid phase value. Importantly,

only a small shift is observed for the C–O stretching modes of the methoxy substituents (1022 to 1034 and 1053 to 1056 cm^{-1}) in all cases, indicating no dissociative adsorption or hydrolysis of DMMP.

To obtain further insight in the adsorption of the DMMP molecule in UiO-66-NH$_2$, periodic static and dynamic density functional theory (DFT) calculations were carried out. The calculations were performed on a UiO-66-NH$_2$ structure containing clusters with isolated missing linker defects (Fig. S8†).[52,53] These simulations reveal two plausible adsorption sites, as shown in Fig. 3d. Firstly, adsorption may occur in a position adjacent to a missing linker in the octahedral cage. In this adsorption site long range interactions occur between the amino groups and the DMMP molecule. Secondly, the DMMP molecule may adsorb directly in the position of a missing linker, where it interacts closely with the water molecules and hydroxides capping the defect sites on the cluster. Both sites show a roughly equal electronic adsorption energy of 100 kJ mol^{-1}.§ To give a view on the mobility of the adsorbate in

the framework, we performed 20 ps molecular dynamics runs at 300 K starting from both adsorption positions. The adsorbate configuration of the DMMP molecules as obtained from static calculations was maintained during the whole simulation, which further underlines the strong adsorption of DMMP on both sites.

High-resolution powder X-ray diffraction patterns of MOF_{DMMP-L} were recorded to localize electron density associated with adsorbed DMMP in the pores of UiO-66-NH$_2$. Rietveld refinement of a framework containing a rigid PO$_4$ tetrahedron as guest model was performed to approximate the position of the central phosphorus atom of the DMMP molecule (Fig. S11 and Table S1, Dataset S1†). Following convergence ($R_{wp} = 3.3\%$), this model fragment is situated on a position (Wyckoff multiplicity 192) in the framework's octahedral cavity (Fig. 3e). In a fully connected UiO-66-NH$_2$ lattice, this PO$_4$ position would overlap with the framework atoms, which supports a correlation between the missing linker defects and the highest affinity adsorption sites. The refined position of the phosphorus site in the octahedral cage complies reasonably well with one of the two adsorption sites obtained by DFT modelling (Fig. S12†). Due to the disordered nature of the missing linkers, it is not possible to conclusively refute the occurrence of the second adsorption site based on X-ray diffraction.

Conclusions

We demonstrated the potential of UiO-66 type MOFs in work function-based sensors for alkyl phosphonate nerve agents. Through Kelvin probe monitoring, the nerve agent simulant DMMP was reversibly detected, both in dry and humid conditions, down to low ppb concentrations. The high sensitivity of UiO-66-NH$_2$ results from a series of confined interactions of DMMP in the octahedral lattice pocket in proximity to missing linker defects. Our study indicates that integration of MOF sensing materials is an interesting pathway for tailoring of ChemFETs to obtain unmatched sensing performances. In addition, our results show that the electrically insulating nature of typical MOFs does not inevitably lead to a limited suitability for field effect and other potentiometric chemical sensors. The available toolbox of MOF design strategies offers a broad perspective for detection of analytes based on different interactions. Moreover, recent progress in computational screening of MOFs for specific adsorption properties and applications can considerably facilitate optimal matching of analytes and sensing materials.[54,55]

Author contributions

I. S., R. A., P. M. V. and R. V. S. developed the concept. I. S. conducted material synthesis and characterization, analyzed the data and drafted the manuscript with guidance from R. A. and D. D. V. B. B., H. R. and N. S. carried out the structure refinement. J. F. M. O. and D. W. performed the KP experiments. J. H. and V. V. S. conducted the DFT calculations. All authors discussed the results, contributed to writing the manuscript and commented on it.

Notes and references

‡ Control experiments showed no signal due to DMMP interaction with the substrate (Fig. S1). Preliminary MOF screening experiments showed a higher signal for UiO-66-NH$_2$ in comparison to a set of other candidates (Fig. S2).

§ The individual enthalpic and entropic contributions and atomic charges for both adsorption sites are given in Tables S1–S3, Fig. S9 and S10.

1 K. Kim, O. G. Tsay, D. A. Atwood and D. G. Churchill, *Chem. Rev.*, 2011, **111**, 5345–5403.
2 L. M. Eubanks, T. J. Dickerson and K. D. Janda, *Chem. Soc. Rev.*, 2007, **36**, 458.
3 National Research Council, *Acute Exposure Guideline Levels for Selected Airborne Chemicals*, vol. 3, Washington, DC: The National Academies Press, 2003 DOI: 10.17226/10672.
4 Y. Tokuda, M. Kikuchi, O. Takahashi and G. H. Stein, *Resuscitation*, 2006, **68**, 193–202.
5 S. C. Lee, H. Y. Choi, S. J. Lee, W. S. Lee, J. S. Huh, D. D. Lee and J. C. Kim, *Sens. Actuators, B*, 2009, **137**, 239–245.
6 R. Yoo, S. Cho, M.-J. Song and W. Lee, *Sens. Actuators, B*, 2015, **221**, 217–223.
7 M. Li, E. B. Myers, H. X. Tang, S. J. Aldridge, H. C. McCaig, J. J. Whiting, R. J. Simonson, N. S. Lewis and M. L. Roukes, *Nano Lett.*, 2010, **10**, 3899–3903.
8 H. J. Lee, K. K. Park, M. Kupnik, ö. Oralkan and B. T. Khuri-Yakub, *Anal. Chem.*, 2011, **83**, 9314–9320.
9 T. H. Stievater, M. W. Pruessner, D. Park, W. S. Rabinovich, R. Andrew McGill, D. A. Kozak, R. Furstenberg, S. A. Holmstrom and J. B. Khurgin, *Opt. Lett.*, 2014, **39**, 969.
10 Y. Long, Y. Wang, X. Du, L. Cheng, P. Wu and Y. Jiang, *Sensors*, 2015, **15**, 18302–18314.
11 W. Zhang, A. M. Asiri, D. Liu, D. Du and Y. Lin, *TrAC, Trends Anal. Chem.*, 2014, **54**, 1–10.
12 G. Korotcenkov, *Handbook of Gas Sensor Materials: Properties, Advantages and Shortcomings for Applications Volume 1: Conventional Approaches*, Springer New York, New York, NY, 2013.
13 J. Janata and M. Josowicz, *Anal. Chem.*, 1997, **69**, 293A–296A.
14 J. Janata, *Electroanalysis*, 2004, **16**, 1831–1835.

15 S. Joo and R. B. Brown, *Chem. Rev.*, 2008, **108**, 638–651.

16 S. Kitagawa, R. Kitaura and S. Noro, *Angew. Chem., Int. Ed.*, 2004, **43**, 2334–2375.

17 H. Furukawa, K. E. Cordova, M. O'Keeffe and O. M. Yaghi, *Science*, 2013, **341**, 1230444.

18 J. Liu, L. Chen, H. Cui, J. Zhang, L. Zhang and C.-Y. Su, *Chem. Soc. Rev.*, 2014, **43**, 6011–6061.

19 Y. He, W. Zhou, G. Qian and B. Chen, *Chem. Soc. Rev.*, 2014, **43**, 5657–5678.

20 J.-R. Li, J. Sculley and H.-C. Zhou, *Chem. Rev.*, 2011, **112**, 869–932.

21 V. Stavila, A. A. Talin and M. D. Allendorf, *Chem. Soc. Rev.*, 2014, **43**, 5994–6010.

22 A. A. Talin, A. Centrone, A. C. Ford, M. E. Foster, V. Stavila, P. Haney, R. A. Kinney, V. Szalai, F. El Gabaly, H. P. Yoon, F. Leonard and M. D. Allendorf, *Science*, 2014, **343**, 66–69.

23 I. Stassen, M. Styles, G. Grenci, H. V. Gorp, W. Vanderlinden, S. D. Feyter, P. Falcaro, D. D. Vos, P. Vereecken and R. Ameloot, *Nat. Mater.*, 2016, **15**, 304–310.

24 I. Stassen, M. Styles, T. Van Assche, N. Campagnol, J. Fransaer, J. Denayer, J.-C. Tan, P. Falcaro, D. De Vos and R. Ameloot, *Chem. Mater.*, 2015, **27**, 1801–1807.

25 L. E. Kreno, K. Leong, O. K. Farha, M. Allendorf, R. P. Van Duyne and J. T. Hupp, *Chem. Rev.*, 2012, **112**, 1105–1125.

26 M. G. Campbell, D. Sheberla, S. F. Liu, T. M. Swager and M. Dincă, *Angew. Chem., Int. Ed.*, 2015, **54**, 4349–4352.

27 M. G. Campbell, S. F. Liu, T. M. Swager and M. Dincă, *J. Am. Chem. Soc.*, 2015, **137**, 13780–13783.

28 Z. Ni, J. P. Jerrell, K. R. Cadwallader and R. I. Masel, *Anal. Chem.*, 2007, **79**, 1290–1293.

29 C. Montoro, F. Linares, E. Quartapelle Procopio, I. Senkovska, S. Kaskel, S. Galli, N. Masciocchi, E. Barea and J. A. R. Navarro, *J. Am. Chem. Soc.*, 2011, **133**, 11888–11891.

30 F.-J. Ma, S. Liu, C. Sun, D.-D. Liang, G. Ren, F. Wei, Y. Chen and Z. Su, *J. Am. Chem. Soc.*, 2011, **133**, 4178–4181.

31 S. Wang, L. Bromberg, H. Schreuder-Gibson and T. A. Hatton, *ACS Appl. Mater. Interfaces*, 2013, **5**, 1269–1278.

32 J. E. Mondloch, M. J. Katz, W. C. Isley III, P. Ghosh, P. Liao, W. Bury, G. W. Wagner, M. G. Hall, J. B. DeCoste, G. W. Peterson, R. Q. Snurr, C. J. Cramer, J. T. Hupp and O. K. Farha, *Nat. Mater.*, 2015, 1–5.

33 Z. Hu and D. Zhao, *Dalton Trans.*, 2015, **44**, 19018–19040.

34 M. J. Katz, J. E. Mondloch, R. K. Totten, J. K. Park, S. T. Nguyen, O. K. Farha and J. T. Hupp, *Angew. Chem.*, 2014, **126**, 507–511.

35 M. J. Schöning and A. Poghossian, *Analyst*, 2002, **127**, 1137–1151.

36 A. D'Amico, C. Di Natale, R. Paolesse, A. Mantini, C. Goletti, F. Davide and G. Filosofi, *Sens. Actuators, B*, 2000, **70**, 254–262.

37 M. J. Schöning and A. Poghossian, *Electroanalysis*, 2006, **18**, 1893–1900.

38 J. Janata and M. Josowicz, *Nat. Mater.*, 2003, **2**, 19–24.

39 M. J. Katz, S.-Y. Moon, J. E. Mondloch, M. H. Beyzavi, C. J. Stephenson, J. T. Hupp and O. K. Farha, *Chem. Sci.*, 2015, **6**, 2086–2091.

40 E. S. Snow, *Science*, 2005, **307**, 1942–1945.

41 X. Du, Z. Wang, J. Huang, S. Tao, X. Tang and Y. Jiang, *J. Mater. Sci.*, 2009, **44**, 5872–5876.

42 K. K. Park, H. Lee, M. Kupnik, Ö. Oralkan, J. P. Ramseyer, H. P. Lang, M. Hegner, C. Gerber and B. T. Khuri-Yakub, *Sens. Actuators, B*, 2011, **160**, 1120–1127.

43 A. Oprea, N. Bârsan and U. Weimar, *Sens. Actuators, B*, 2009, **142**, 470–493.

44 P. Davydovskaya, R. Pohle, A. Tawil and M. Fleischer, *Sens. Actuators, B*, 2013, **187**, 142–146.

45 P. Davydovskaya, A. Ranft, B. V. Lotsch and R. Pohle, *Anal. Chem.*, 2014, **86**, 6948–6958.

46 M. F. de Lange, K. J. F. M. Verouden, T. J. H. Vlugt, J. Gascon and F. Kapteijn, *Chem. Rev.*, 2015, **115**, 12205–12250.

47 A. B. Butrow, J. H. Buchanan and D. E. Tevault, *J. Chem. Eng. Data*, 2009, **54**, 1876–1883.

48 S. Fanget, S. Hentz, P. Puget, J. Arcamone, M. Matheron, E. Colinet, P. Andreucci, L. Duraffourg, E. Myers and M. L. Roukes, *Sens. Actuators, B*, 2011, **160**, 804–821.

49 C. Zimmermann, P. Mazein, D. Rebiere, C. Dejous, J. Pistre and R. Planade, *IEEE Sens. J.*, 2004, **4**, 479–488.

50 L. Valenzano, B. Civalleri, S. Chavan, S. Bordiga, M. H. Nilsen, S. Jakobsen, K. P. Lillerud and C. Lamberti, *Chem. Mater.*, 2011, **23**, 1700–1718.

51 V. M. Bermudez, *Langmuir*, 2010, **26**, 18144–18154.

52 S. Grimme, J. Antony, S. Ehrlich and H. Krieg, *J. Chem. Phys.*, 2010, **132**, 154104.

53 J. Hajek, M. Vandichel, B. Van de Voorde, B. Bueken, D. De Vos, M. Waroquier and V. Van Speybroeck, *J. Catal.*, 2015, **331**, 1–12.

54 Y. J. Colón and R. Q. Snurr, *Chem. Soc. Rev.*, 2014, **43**, 5735–5749.

55 F.-X. Coudert and A. H. Fuchs, *Coord. Chem. Rev.*, 2016, **307**, 211–236.